Constraints on the magnitude and rate of CO_2 dissolution at Bravo Dome natural gas field

Kiran J. Sathaye[a], Marc A. Hesse[a,b,1], Martin Cassidy[c], and Daniel F. Stockli[a]

[a]Department of Geological Sciences, Jackson School of Geosciences, University of Texas at Austin, Austin, TX 78712; [b]Institute of Computational Engineering and Sciences, University of Texas at Austin, Austin, TX 78712; and [c]Department of Earth and Atmospheric Sciences, University of Houston, Houston, TX 77204

Edited by Susan L. Brantley, Pennsylvania State University, University Park, PA, and approved September 12, 2014 (received for review April 4, 2014)

The injection of carbon dioxide (CO_2) captured at large point sources into deep saline aquifers can significantly reduce anthropogenic CO_2 emissions from fossil fuels. Dissolution of the injected CO_2 into the formation brine is a trapping mechanism that helps to ensure the long-term security of geological CO_2 storage. We use thermochronology to estimate the timing of CO_2 emplacement at Bravo Dome, a large natural CO_2 field at a depth of 700 m in New Mexico. Together with estimates of the total mass loss from the field we present, to our knowledge, the first constraints on the magnitude, mechanisms, and rates of CO_2 dissolution on millennial timescales. Apatite (U-Th)/He thermochronology records heating of the Bravo Dome reservoir due to the emplacement of hot volcanic gases 1.2–1.5 Ma. The CO_2 accumulation is therefore significantly older than previous estimates of 10 ka, which demonstrates that safe long-term geological CO_2 storage is possible. Integrating geophysical and geochemical data, we estimate that 1.3 Gt CO_2 are currently stored at Bravo Dome, but that only 22% of the emplaced CO_2 has dissolved into the brine over 1.2 My. Roughly 40% of the dissolution occurred during the emplacement. The CO_2 dissolved after emplacement exceeds the amount expected from diffusion and provides field evidence for convective dissolution with a rate of 0.1 g/(m^2y). The similarity between Bravo Dome and major US saline aquifers suggests that significant amounts of CO_2 are likely to dissolve during injection at US storage sites, but that convective dissolution is unlikely to trap all injected CO_2 on the 10-ky timescale typically considered for storage projects.

geological carbon storage | thermochronology | noble gases | porous media convection | carbon sequestration

Carbon capture and storage has been identified as a potential technology for reductions in carbon dioxide (CO_2) emissions from coal- and natural gas-fired power plants. CO_2 that would otherwise be released into the atmosphere is captured at power plants and injected into porous geological formations for permanent storage. Carbon capture and storage has the potential for significant reductions of anthropogenic CO_2 emissions, because deep saline aquifers provide large storage volumes (1, 2) and existing operations have demonstrated that CO_2 injection and monitoring in saline aquifers are feasible (3).

The leakage of CO_2 from the storage formation into potable aquifers or back into the atmosphere is an inherent risk of large-scale geological CO_2 storage (4–6). Long-term storage security is therefore enhanced by physical and chemical processes that increasingly trap the injected CO_2 in the subsurface over time. Injected CO_2 can be trapped by capillary forces through the formation of disconnected ganglia or by precipitation as solid phases (7–9). Dissolution of CO_2 into the brine not only is a required first step for the subsequent permanent trapping in stable minerals, but also is considered a trapping mechanism itself. The density of the brine increases with dissolved CO_2 concentration and therefore forms a stable stratification less susceptible to leakage (10). Here we refer to total dissolved inorganic carbon simply as dissolved CO_2. The carbon isotope composition of most natural CO_2 fields indicates that dissolution of CO_2 into the brine is often the dominant trapping process over millennial timescales (11). Determining the rates of CO_2 dissolution is therefore an important aspect of geological CO_2 storage and it has been the focus of intense research in the last decade.

Over the timescales of hydrologic processes the reaction kinetics are fast (12), so that the rate of CO_2 dissolution is limited by interfacial area and mass transport. The uncertainty in the dissolution rate is large, because geological heterogeneity determines the interfacial area and because mass transport can either be diffusive and slow or advective and potentially fast (13). Advective mass transport and fast dissolution always occur during injection and the interfacial area continuously increases as CO_2 contacts new unsaturated brine. The total amount of CO_2 that can be dissolved during injection is determined by the amount of brine inside the CO_2 plume and the migration distance of the plume. After the CO_2 plume has ponded in a geological structure, dissolution into the brine will continue across the gas–water contact and may eventually lead to complete disappearance of the CO_2 plume (14). It is therefore this latter stage of dissolution that ensures long-term storage security, if the CO_2 has ponded.

At this stage, dissolution is limited by the mass transport of dissolved CO_2 away from the gas–water contact. Advective mass transport is possible, if the increase in brine density with aqueous CO_2 concentration destabilizes the diffusive boundary layer beneath the gas–water contact and induces convective overturn in the brine (10, 13, 15). It is therefore necessary to understand the occurrence and rate of convective overturn in the brine, which are determined by the balance of advective and diffusive mass transport, expressed by the Rayleigh number (16, 17). Most work on convective CO_2 dissolution has focused on idealized homogeneous

Significance

Carbon capture and geological storage allow immediate and significant reductions in CO_2 emissions from fossil fuels. CO_2 dissolution into saline water enhances long-term storage security, but dissolution rates are too slow to be quantified during injection pilots. Therefore, we estimate dissolution rates over millennial timescales at the Bravo Dome gas field, a natural analog for geological CO_2 storage. We show that 1.6 Gt CO_2 have been stored at Bravo Dome since the beginning of CO_2 emplacement 1.2–1.5 Ma. Approximately 10% of the CO_2 dissolved during its emplacement, while another 10% dissolved into the underlying aquifer. This exceeds the amount expected from diffusion and provides field evidence for convective CO_2 dissolution. The convective dissolution rate, however, is slow in typical US aquifers.

Author contributions: M.A.H. designed research with contributions from M.C.; K.J.S., M.C., and D.F.S. performed research; K.J.S. and D.F.S. analyzed data; and K.J.S. and M.A.H. wrote the paper.

The authors declare no conflict of interest.

This article is a PNAS Direct Submission.

Freely available online through the PNAS open access option.

[1]To whom correspondence should be addressed. Email: mhesse@jsg.utexas.edu.

This article contains supporting information online at www.pnas.org/lookup/suppl/doi:10.1073/pnas.1406076111/-/DCSupplemental.

systems and large Rayleigh numbers, where convection occurs after an initial incubation time (13, 18–20) and the ratio of the convective to the diffusive dissolution rate is a power law of the Rayleigh number (15, 21–24). It is not clear, however, how this work relates to highly heterogeneous natural formations, where already the definition of an appropriate Rayleigh number is difficult (25) and numerical simulations show that simple patterns of heterogeneity strongly affect the convective flux (26, 27).

It is therefore necessary to constrain the magnitude and rate of CO_2 dissolution directly from measurements in the field. The convective dissolution rate, however, is too slow to be quantified during pilot or commercial projects on timescales of a few decades. Therefore, we have studied CO_2 dissolution over millennial timescales in a natural CO_2 field that provides an analog for the long-term evolution of a geological storage site. We present the first constraints on the magnitude and average rate of convective CO_2 dissolution based on field data.

The Bravo Dome natural gas field in New Mexico provides unique constraints on CO_2 dissolution in the field, because the combination of large-scale commercial development and decades of geochemical research has produced a comprehensive and detailed dataset. Fig. 1*A* shows the location and extent of the Bravo Dome natural gas field, which covers 3,600 km^2. Below we show that the reservoir held 1.3 Gt of natural gas before the beginning of production in 1981. The composition of the gas is 99.8% CO_2, 0.1% N_2, with traces of light hydrocarbons and noble gases. The total dissolved solids in the reservoir brine are 85,000 mg/L (28). The reservoir is formed by a structural–stratigraphic trap on a structural high, dipping to the southeast and segmented by several faults, as shown in the cross section in Fig. 1*C*. The reservoir is in the Permian Tubb sandstone, which rests unconformably on Precambrian basement and is sealed by the overlying Cimarron Anhydrite. The Tubb consists of well-sorted arkosic riverine sandstones embedded in a matrix of silty aeolian deposits, which leads to a strongly bimodal distribution of porosity, ϕ. The reservoir thins and the abundance of sand decreases toward the west, away from the sediment source in the Ancestral Rocky Mountains in the east (29–31).

The isotopic composition of the noble gases and carbon at Bravo Dome and their gradients across the field have received considerable attention (32–37). The high ^3He content of the gas indicates that it is of volcanic origin (33, 35) and provides an important conservative tracer to evaluate local CO_2 dissolution based on changes in the $CO_2/^3He$ ratio across the field. The decrease in $CO_2/^3He$ from $5.35{\cdot}10^9$ in the west to $2.25{\cdot}10^9$ in the east suggests that locally more than half the emplaced CO_2 must have dissolved (11, 37, 38). The reservoir shows little sign of permanent CO_2 trapping in the form of carbonate precipitation (39, 40), suggesting CO_2 dissolution is the dominant trapping mechanism.

Fig. 1*A* shows a pronounced maximum of the 1981 reservoir pressure (29) that suggests continued charging of the western part of the reservoir from fractures in the basement. The initial emplacement of the gas likely also occurred in this area and subsequently filled the reservoir down-dip, forming an elongated gravity tongue (41). This scenario is supported by the increase in groundwater-derived ^{20}Ne in the gas from west to east (37). In 1994 the gas–water contact was determined to be horizontal within each segment of the reservoir, but offset across the faults segmenting the reservoir (38, 42).

Below we provide to our knowledge the first constraints on the magnitude, the mechanism, and the rate of CO_2 dissolution at Bravo Dome. First we provide new thermochronological constraints on the age of the reservoir. Then we determine the mass of CO_2 dissolved by combining existing geophysical and geochemical data. Finally, we estimate the amount of CO_2 dissolved into the residual brine during the emplacement and an averaged dissolution rate for the additional CO_2 that must have dissolved after the ponding of the CO_2 plume.

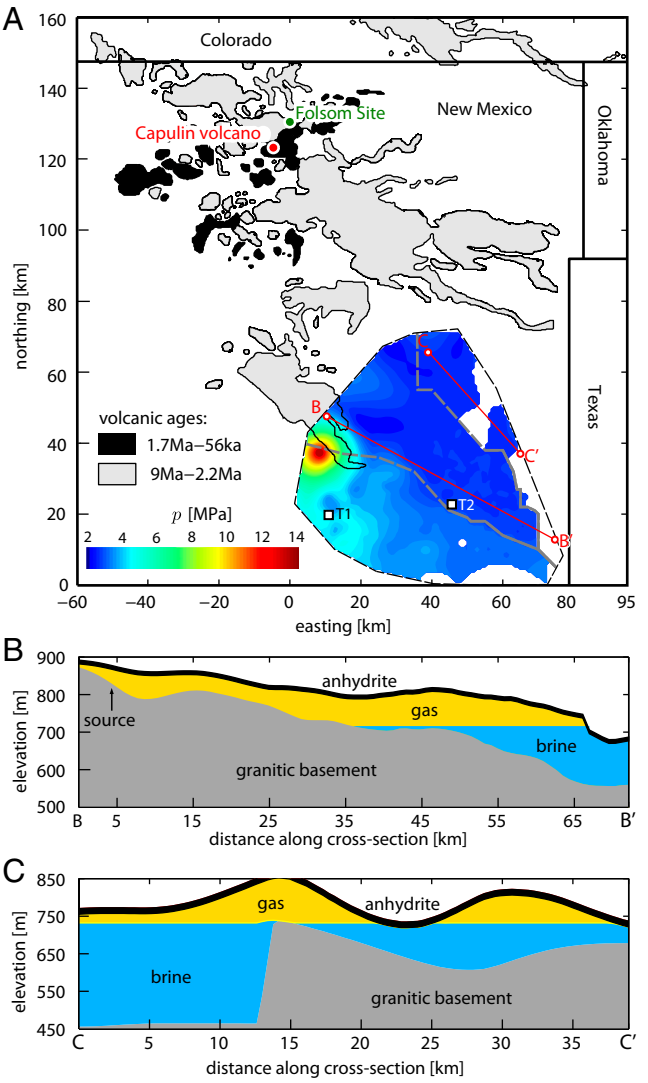

Fig. 1. (*A*) Map showing the location of the Bravo Dome CO_2 field and extrusive products of volcanic activity during the last 9 My. The color map shows the pressure distribution in the gas field in 1981, the squares shows the locations of the samples used for the (U-Th)/He thermochronology, and the locations of the cross sections are indicated in red. Major faults are indicated by gray lines. (*B*) A down-dip cross section of the main section of the reservoir from *B* to *B′*. (*C*) A cross section of the NE segment of the reservoir from *C* to *C′*.

Constraints on the Emplacement Age of Bravo Dome

Any estimate of the CO_2 dissolution rate at Bravo Dome requires a constraint on the age of the initial CO_2 emplacement. All previous studies assume that the emplacement of volcanic gas is contemporaneous with the occurrence of extrusive volcanism in the area (11, 37–40). The commonly cited age for Bravo Dome is 8–10 ky, which is associated with an early radiocarbon date of a campfire at the Folsom archeological site near Capulin Volcano (43), shown in Fig. 1*A*. However, later a comprehensive study of the volcanic geochronology of the area established ages between 56 ky and 1.7 My for the basalts associated with the Capulin stage (44, 45). Here, we present a different approach to constrain the age of the initial CO_2 emplacement. Given that the gas is of volcanic origin and that it was emplaced directly from the basement into the reservoir, the gas is likely to have heated the reservoir above the apatite closure temperature of roughly 75 °C (46) in the vicinity of the entry point.

Table 1. Apatite (U-Th)/He results

No.	Location	Distance from source, km	Age, My
1	T1	17	1.2 ± 0.1
2	T1	17	1.4 ± 0.1
3	T1	17	1.5 ± 0.1
4	T1	17	1.2 ± 0.1
5	T2	34	13.2 ± 0.8
6	T2	34	12.0 ± 0.7
7	T2	34	16.3 ± 1.0
8	T2	34	16.7 ± 1.0

To test this hypothesis, we have analyzed two core samples from the Tubb sandstone in the Bravo Dome wells State HN #1 (103.7965°W, 35.8498°N) and Heimann #2 (103.4128°W, 35.9029°N), shown in Fig. 1 and labeled T1 and T2, respectively. The results of (U-Th)/He thermochronology are shown in Table 1. The samples T1 and T2 are located 17 km and 34 km from the assumed CO_2 source near the pressure maximum in Fig. 1*A*. Zircons show ages between 280 My and 393 My, consistent with the assumed sediment source of the Tubb sandstone in the Ancestral Rocky Mountains (31). Apatites from T2 show ages between 12 My and 17 My consistent with Cenozoic heating due to the migration of hydrothermal fluids (47). In contrast, apatite ages from T1, the sample closer to the CO_2 source, are between 1.2 My and 1.5 My and indicate a localized thermal event that is contemporaneous with the volcanism of the Capulin stage. We suggest that the heating of the reservoir in the vicinity of the CO_2 source is associated with the entry of hot volcanic CO_2 and therefore dates the beginning of the emplacement of CO_2 into the Bravo Dome reservoir between 1.2 Ma and 1.5 Ma. Specific measurements of radioactive and radiogenic isotope concentrations in each crystal are shown in *SI Text*, section 5.

Estimate of the Magnitude of CO_2 Dissolution

Previous authors suggest that no CO_2 leakage to the surface or into the shallow groundwater occurs at Bravo Dome (48) and that mineralization of CO_2 in the reservoir appears to be negligible (39, 40). Changes in CO_2 mass are therefore mainly due to dissolution. Previous work has used the $CO_2/^3He$ ratio in combination with Rayleigh fractionation to infer the local mass fraction of CO_2 that has dissolved (11, 37, 38),

$$\mathcal{F} = \frac{m_f}{m_t}, \qquad [1]$$

where m_t is the total mass of CO_2 per unit area emplaced and m_f is the final mass of CO_2 per unit area in 1981, just before the start of significant commercial production (29). This allows us to infer the local mass loss from the reservoir, given by the local change in CO_2 mass per unit area,

$$\Delta m = m_t - m_f = \left(\frac{1}{\mathcal{F}} - 1\right) m_f, \qquad [2]$$

and the total change of CO_2 mass across the entire field,

$$\Delta M = \iint \Delta m \, dxdy, \qquad [3]$$

where the boundary of the domain of integration is the dashed black line in Fig. 1*A*. This estimate requires only the local fraction of CO_2 dissolved, $\mathcal{F}$, and the final distribution of CO_2 in the reservoir, m_f. Bravo Dome is an ideal site, because geochemical studies have determined gradients of $\mathcal{F}$ across the field and the data from large-scale commercial development constrain the CO_2 distribution, m_f. In the calculations below all point measurements are interpolated across the field, using the Kriging algorithm after removing the regional dipping trend (49). The standard deviations of estimated quantities are computed by propagating the Kriging variance of the interpolated fields through Eqs. **1**–**4**. Details of the variograms and the error propagation are in *SI Text*, section 1.

The Distribution of CO_2 in 1981. The mass of CO_2 per unit area in the reservoir depends on the height of the gas column, h, the gas density, ρ_g, and the volume fraction of the gas, $\phi_f = \phi s_g$, which depends on the porosity of the rock, ϕ, and the saturation of the gas, s_g. Given the large aspect ratio of the reservoir (300:1) we approximate the final mass per unit area in 1981 as

$$m_f = \int_{z_c}^{z_c+h} \phi_g \rho_g \, dz \approx h \overline{\phi}_g \overline{\rho}_g, \qquad [4]$$

where z_c is the elevation of the gas water contact, and $\overline{\phi}_g$ and $\overline{\rho}_g$ are the vertically averaged properties in the gas cap.

The spatial variation of the gas column height, h, is shown in Fig. 2*A* and estimated from the reservoir geometry and the height of the gas–water contact. The reservoir geometry has been obtained from more than 300 well logs, similar to those shown in Fig. 2 *B* and *C*. Both the top and the base of the reservoir have significant topography, which induces large lateral variations in h. Generally, h is largest in the center of the field near the up-dip edge of the gas–water contact, and discontinuities in h are due to offsets of the gas–water contact across faults (42).

The spatial variation of the average gas volume fraction, $\overline{\phi}_g$, is shown in Fig. 3*C* and estimated from more than 3,500 porosity measurements in 36 cored wells (Fig. 3*G*) and 44 mercury injection capillary pressure measurements on core plugs obtained from 4 Bravo Dome wells. The distribution of the CO_2 within the reservoir is controlled by capillary forces, which require larger pressures for nonwetting phases like CO_2 to enter finer-grained rocks with smaller pore sizes. This is illustrated by three representative capillary pressure curves from Bravo Dome shown in Fig. 3*A*. The capillary entry pressure in the fine-grained low-porosity siltstones is so high that CO_2 saturations are insignificant in the pressure range encountered in the reservoir.

In contrast, the coarse-grained, well-sorted, and porous sandstones have low CO_2 entry pressures and allow large CO_2 saturations even at moderate pressures. Fig. 3*B* shows that there is a good correlation between the porosity and the maximum CO_2 saturation, which allows an estimate of the gas volume fraction from the porosity. The large-scale distribution of free-phase CO_2 is therefore controlled by the distribution of the porosity and in particular the occurrence of sandstones within the reservoir.

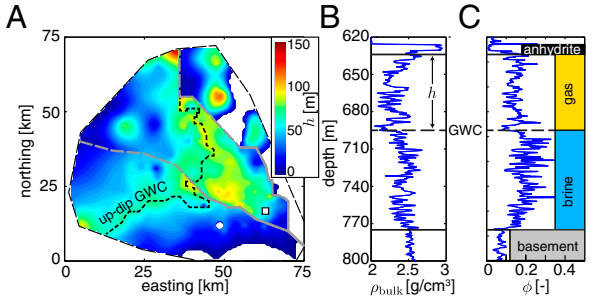

Fig. 2. (*A*) Map of the gas column height, h, throughout the reservoir based on the analysis of 322 well logs and the depth of the gas–water contact (GWC). The up-dip end of the gas–water contact is indicated by a black dashed line. (*B* and *C*) Density (*B*) and neutron porosity (*C*) logs for a typical Bravo Dome well, shown as a square on the map.

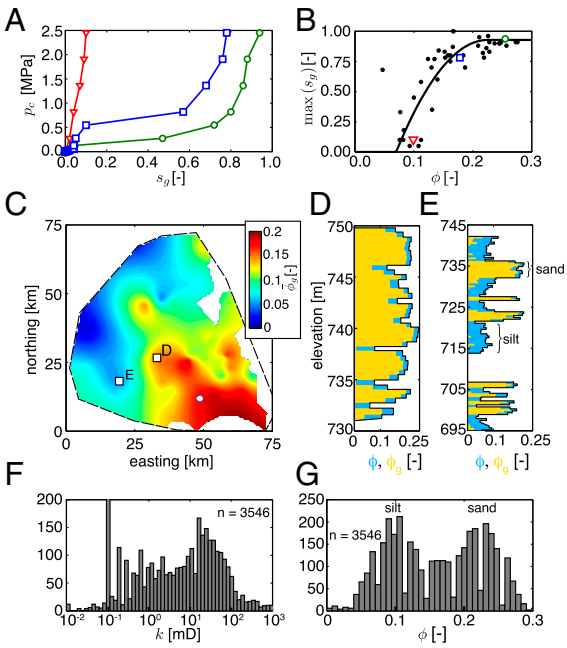

Fig. 3. (*A*) Typical capillary pressure, p_c, curves for Bravo Dome from well Culbertson 1. Measurements have been converted from mercury–air to brine–gas (50). (*B*) Maximum CO_2 saturations from 44 p_c curves as function of porosity. (*C*) Map of the vertically averaged gas volume fraction, $\overline{\phi}_g$, throughout the reservoir. (*D*) Vertical porosity variation at well Culbertson 1. (*E*) Vertical porosity variation at well State FM#1. Both wells are shown as squares on the map and ϕ_g is estimated from the relation in plot *B*. *F* and *G* show histograms of all available k (gas) and ϕ measurements from Bravo Dome, respectively.

The porosity distribution is constrained by frequent measurements of the porosity along 36 cored wells; two examples are shown in Fig. 3 *D* and *E*. Sandstones are less frequent in the west, reflecting a general proximal to distal depositional trend in the reservoir (31). Using the correlation between porosity and gas saturation from Fig. 3*B*, we obtain the vertical profiles of gas volume fraction in 40 wells. The vertically averaged gas volume fraction, $\overline{\phi}_g$, in Fig. 3*C* illustrates the control that the abundance of sandstones has on the distribution of CO_2 within Bravo Dome.

The gas density is a function of the reservoir pressure, p, and temperature, T. Temperature logs are nearly constant throughout the reservoir at 30 °C, so that the spatial variation of the gas density, ρ_g, reflects the pattern in the bottom-hole pressure in 1981, shown in Fig. 1*A*. To compute the density we assume that the gas pressure is uniform throughout a vertical column and then interpolate between established data (51). We note that the CO_2 is gaseous throughout most of the reservoir and becomes supercritical only near the pressure maximum in the west.

Given the maps of gas thickness in Fig. 2*C*, the gas volume fraction in Fig. 3*C*, and the gas density in Fig. 1*A*, the final CO_2 mass per unit area in 1981 can be computed from Eq. **4** and is shown in Fig. 4*A*. The total amount of CO_2 stored at Bravo Dome in 1981 obtained from our calculation is 1.3 ± 0.6 Gt CO_2 or ~22.7 trillion cubic feet.

Local Fraction of CO_2 Dissolved. Previous work has used the variation of the $CO_2/^3He$ ratio from $5.35{\cdot}10^9$ to $2.25{\cdot}10^9$ to conclude that more than half of the CO_2 has dissolved locally in the vicinity of the depleted measurement (11, 37, 38). These estimates are based on the assumption of Rayleigh fractionation between a gas of constant initial $CO_2/^3He$ ratio of $5.35{\cdot}10^9$ and brine. ^3He is almost two orders of magnitude less soluble in water than CO_2 (52), so that 99% of ^3He remains in the gas and it can be thought of as a conservative tracer (53) (*SI Text*, section 2). In this limit, the local fraction of CO_2 dissolved is simply given by

$$\mathcal{F} \approx 1 - \frac{[CO_2/^3He]_f}{[CO_2/^3He]_i}, \qquad [5]$$

where $[CO_2/^3He]_i = 5.35 \cdot 10^9$ is the initial ratio of the volcanic gas emplaced into Bravo Dome and $[CO_2/^3He]_f$ is the current ratio measured in previous studies (11, 37, 38).

The spatial variation of the local fraction of CO_2 dissolved, $\mathcal{F}$, is shown in Fig. 4*B*. By definition, $\mathcal{F} = 0$ at the location of the highest $CO_2/^3He$ ratio in the west and the fraction of CO_2 dissolved generally increases toward the down-dip gas–water contact of the reservoir. The close spatial association of the smallest fraction of CO_2 dissolved with highest pressures in the reservoir supports the hypothesis that the gas entered Bravo Dome in this area and that CO_2 increasingly dissolved as it filled the reservoir from west to east. The largest fraction of the emplaced CO_2 has dissolved in the northeastern segment of Bravo Dome, where the reservoir is much thicker because the basement has been lowered by faulting (Fig. 1*C*).

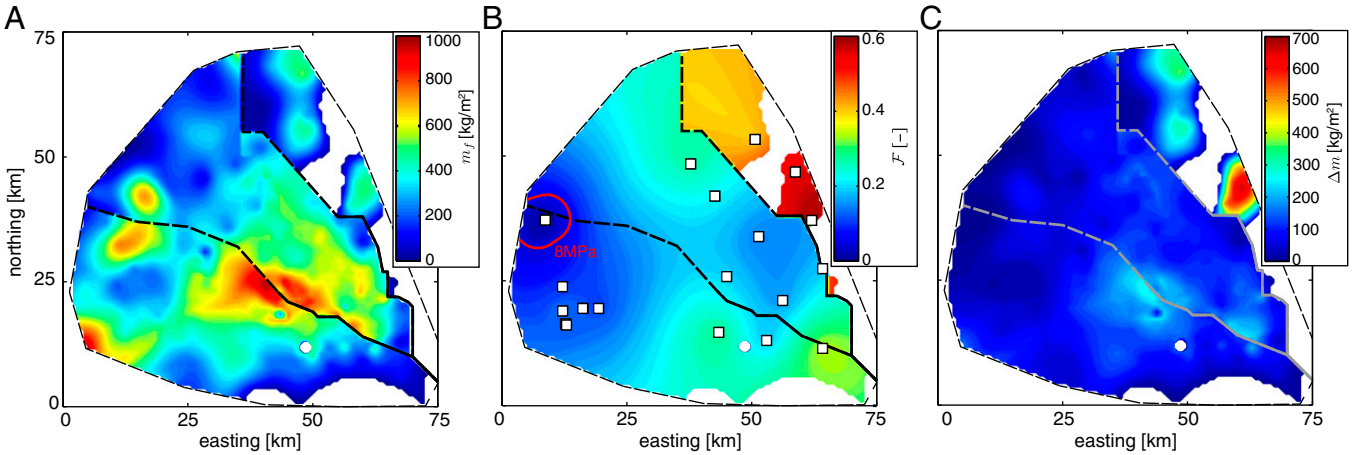

Fig. 4. (*A*) Map of the CO_2 distribution in the reservoir in terms of the mass of CO_2 per unit area in 1981, m_f. (*B*) Map of the local fraction of CO_2 dissolved assuming Rayleigh fractionation, $\mathcal{F}$. The red line is the 8-MPa pressure contour from Fig. 1*A* that indicates the likely location of the CO_2 source. (*C*) Map of the local change in the mass of CO_2 per unit area, Δm.

Fig. 4*C* shows the distribution of the mass loss, Δm, in the reservoir. Due to the highly variable distribution of CO_2 within the reservoir, the variation of Δm is different from $\mathcal{F}$, in particular near the gas–water contact where Δm approaches zero although $\mathcal{F}$ is generally large. This is simply due to the small initial mass of CO_2 per unit area near the gas–water contact and illustrates the importance of considering the distribution of CO_2 in dissolution calculations. Again the northeastern segment of the reservoir shows the largest mass loss from the reservoir.

Using Eq. **3**, the total mass of CO_2 that has been lost from Bravo Dome due to dissolution, ΔM, is 366 ± 120 Mt CO_2, roughly equivalent to the amount of CO_2 emitted by a typical 500-MW coal power plant over a 75-y period (54). Adding this to the mass of CO_2 in Bravo Dome in 1981 the total mass of CO_2 emplaced into Bravo Dome is 1.6 ± 0.67 Gt CO_2. Therefore, only 22 ± 7% of the emplaced CO_2 has dissolved, significantly less than maximum local estimates of more than 50% (11, 37, 38). The uncertainty in this dissolution estimate is mostly due to the large variance in the top and bottom elevations of the reservoir rather than the sparsity of ^{3}He measurements, which have a low total variance.

Discussion

We have presented a novel application of thermochronology to date the emplacement of CO_2 into Bravo Dome and to our knowledge the first field-based estimates of the mass of CO_2 dissolved over millennial timescales in a saline aquifer. Together, the data presented have the potential to constrain the rate of CO_2 dissolution, in particular the rate of convective CO_2 dissolution, in real geological formations over long timescales that are not directly accessible to observation. Estimates of dissolution rates in the field provide important information for the assessment of the long-term security of geological CO_2 storage. Before we present an estimate of dissolution rate we first discuss whether the assumption underlying the age estimate is reasonable and how much CO_2 is likely to have dissolved during the initial emplacement.

Reservoir Heating. The resetting of thermochronometers is usually associated with burial and exhumation. At Bravo Dome the erosion in the last 1 My is only a few meters (45) and can therefore not account for the temperature changes required to reset the apatites. Similarly, the absence of a substantial magma chamber within a few kilometers of Bravo Dome makes regional heating due to a magmatic intrusion unlikely (*SI Text*, section 3). The 15-My difference in apatite ages between samples separated by 17 km suggests that the heating event at 1.2 Ma to 1.5 Ma must be local. We therefore propose that the heating is due to injection of hot volcanic CO_2. This requires that the injected CO_2 has enough energy to heat the reservoir from 30 °C to above the closure temperature of apatite at 75 °C. A simple energy balance shows that this is reasonable (*SI Text*, section 3). Assuming radial flow from the pressure maximum to the sampling location a volume of $2.2{\cdot}10^{10}$ m^3 has to be heated by at least 50 °C. Likely the heating was localized to the sandbodies invaded by the hot CO_2. In this case, the CO_2 must have entered with an average temperature of at least 400 °C, well within the temperature range observed for volcanic gases at the surface. It is therefore plausible that the emplacement of hot volcanic CO_2 heated the reservoir sufficiently to exceed the apatite closure temperature.

Dissolution During Emplacement. Due to the low average gas saturation throughout the reservoir (Fig. 3*C*), substantial amounts of CO_2 can be dissolved into the brine that is currently contained within the gas cap. This brine resides in the siltstones where high entry pressures prevent the invasion of CO_2. During emplacement CO_2 enters the sandstones and dissolved CO_2 has to migrate into the low-permeability siltstones by diffusion. The porosity logs in Fig. 3 *D* and *E* show that the average thickness of the siltstones is less than 10 m, so that diffusive transport can saturate the siltstones in 5 ky. Therefore, we consider all CO_2 dissolved in this way to occur during or shortly after emplacement. We estimate the equilibrium concentration of dissolved CO_2 in the brine from the 1981 pressures, assuming a 2-M NaCl brine (55). Of 266 Mt CO_2 dissolved in the main part of the reservoir ~50% (142 Mt CO_2) dissolved during emplacement. Of 100 Mt CO_2 dissolved in the northeastern (NE) segment ~14% dissolved during emplacement.

Rate of Convective Dissolution. Significant dissolution after CO_2 emplacement occurred in both parts of the reservoir, in particular in the NE segment of the reservoir, where 86% of the dissolution occurred after emplacement. Diffusive mass transport downward from the gas–water contact over 1.4 My can account for the dissolution of less than 0.1 Mt CO_2. This provides field evidence for the acceleration of dissolution either by background flow in the aquifer or by buoyancy-driven convection. Assuming that the brine was fully saturated with CO_2, convection must have moved a brine volume of $7 \cdot 10^9$ m^3 to dissolve the additional CO_2. This corresponds to ~25% of the reservoir brine below the gas–water contact and suggests local buoyancy-driven flow rather than regional background flow in the aquifer. Convection occurs if the Rayleigh number exceeds a critical value

$$\mathrm{Ra} = \frac{k\Delta\rho g H}{\phi \mu D} > \mathrm{Ra}_c, \qquad [6]$$

where $\Delta\rho$ is the density change of the brine, μ is the brine viscosity, H is the thickness of the brine, and D is the aqueous diffusion coefficient of CO_2. In heterogeneous reservoirs it is difficult to define a suitable mean permeability, $\bar{k}$, and we use the geometric mean for each cored well. Estimates of Ra for the NE segment are below 20 and therefore the same order of magnitude as Ra_c in simple porous media (17). Given the additional perturbations provided by heterogeneity and complex geometry, buoyancy-driven convection is possible in the NE segment, but the expected convective flux is small for $\mathrm{Ra} \approx \mathrm{Ra}_c$.

Assuming continuous convective dissolution of 86 Mt CO_2 since the emplacement 1.2 Ma ago, the average dissolution rate in the NE segment is 70 t/y, consistent with the small Ra. Normalizing the rate by the 623 km^2 of the gas–water contact in the NE segment, the average flux is only 0.1 g/(m^{2}y). This is likely due to the low permeabilities at Bravo Dome (Fig. 3*F*) and the strong geological heterogeneity, where permeable sandstones are embedded in a low-permeability matrix of siltstone. In this case, the connectivity of the individual sandbodies is likely crucial in determining the rate of convective overturn. Given that only 25% of the brine immediately available beneath the gas–water contact has been saturated with CO_2, it is unlikely that the low average dissolution rates can be explained by convective shutdown (22, 56) or limitations due to the lateral migration of dissolved CO_2 as a dense gravity current (14, 57).

Implications for Geological CO_2 Storage

Our results show that 1.3 Gt CO_2 have been safely contained at Bravo Dome at a depth of 700 m for more than 1 My without any detectable CO_2 leakage to the surface. This demonstrates that safe geological storage of very large accumulations of CO_2 is possible in suitable geological structures. In contrast to many studies that suggest timescales less than 10 ky for the dissolution trapping, we show that over 1 My only ~20% of the emplaced CO_2 has dissolved.

Our results highlight the importance of dissolution during CO_2 emplacement, which likely accounts for more than 40% of the dissolution trapping at Bravo Dome. This mechanism is favored in highly heterogeneous reservoirs, where large volumes of brine are left behind the advancing CO_2 front. In engineered storage sites the timescale for this dissolution would be the injection period plus the time for diffusive equilibration, which depends on the length scale of the geological heterogeneity. A suitable description of the

geological heterogeneity of the storage site is therefore essential to predict the magnitude of dissolution during emplacement.

Our estimates show that significant amounts of additional dissolution are required, in particular in the NE segment of Bravo Dome, to explain the geochemical observations. This provides indirect field evidence for convective dissolution of CO_2 on millennial timescales. The estimated average rate of convective dissolution at Bravo Dome is only 0.1 g/(m^2y), consistent with the low Rayleigh numbers at Bravo Dome. This contrasts with the large fluxes of ∼20 kg/(m^2y) that have been estimated for the highly permeable Sleipner storage site in the North Sea (15).

A recent survey of deep saline aquifers in the continental United States (2) shows that Rayleigh numbers below 20 are typical (*SI Text*, section 4.2). Bravo Dome may therefore provide a useful analog for the low-permeability storage sites common in the United States. In these storage sites dissolution during emplacement will be dominant and convective dissolution fluxes after emplacement are negligible on the 10-ky timescale typically envisioned for engineered storage sites.

ACKNOWLEDGMENTS. The authors thank Albert Giussani of Occidental Petroleum for sharing the initial bottom hole pressures of Bravo Dome. The authors also thank Vyetta Jordan of the Oklahoma Geological Survey for her help in locating the data and cores from Bravo Dome. This work was supported as part of the Center for Frontiers of Subsurface Energy Security, an Energy Frontier Research Center, funded by the US Department of Energy, Office of Science, Office of Basic Energy Sciences, Materials Sciences and Engineering Division under Award DE-SC0001114.

1. Orr FM, Jr (2009) CO_2 capture and storage: Are we ready? *Energy Environ Sci* 2(5):449–458.
2. Szulczewski ML, MacMinn CW, Herzog HJ, Juanes R (2012) Lifetime of carbon capture and storage as a climate-change mitigation technology. *Proc Natl Acad Sci USA* 109(14):5185–5189.
3. Michael K, et al. (2010) Geological storage of CO_2 in saline aquifers. A review of the experience from existing storage operations. *Int J Greenh Gas Control* 4(4):659–667.
4. Gasda SE, Bachu S, Celia Ma (2004) Spatial characterization of the location of potentially leaky wells penetrating a deep saline aquifer in a mature sedimentary basin. *Environ Geol* 46(6–7):707–720.
5. Roberts JJ, Wood RA, Haszeldine RS (2011) Assessing the health risks of natural CO_2 seeps in Italy. *Proc Natl Acad Sci USA* 108(40):16545–16548.
6. Trautz RC, et al. (2013) Effect of dissolved CO_2 on a shallow groundwater system: A controlled release field experiment. *Environ Sci Technol* 47(1):298–305.
7. Bachu S, Gunter W, Perkins E (1994) Aquifer disposal of CO_2: Hydrodynamic and mineral trapping. *Energy Convers Manage* 35(4):269–279.
8. Kumar A, et al. (2005) Reservoir simulation of CO2 storage in deep saline aquifers. *SPE J* 10(3):17–21.
9. Balashov VN, Guthrie GD, Hakala AJ, Lopano CL, Rimstidt JD, Brantley SL (2013) Predictive modeling of CO2 sequestration in deep saline sandstone reservoirs: Impacts of geochemical kinetics. *Appl Geochem* 30:41–56.
10. Weir G, White S, Kissling W (1996) Reservoir storage and containment of greenhouse gases. *Transp Porous Media* 23(1):37–60.
11. Gilfillan SMV, et al. (2009) Solubility trapping in formation water as dominant $CO(_2)$ sink in natural gas fields. *Nature* 458(7238):614–618.
12. Mitchell MJ, Jensen OE, Cliffe KA, Maroto-Valer MM (2009) A model of carbon dioxide dissolution and mineral carbonation kinetics. *Proc R Soc Math Phys Eng Sci* 466(2117):1265–1290.
13. Ennis-King J, Paterson L (2005) Role of convective mixing in the long-term storage of carbon dioxide in deep saline formations. *SPE J* 10(3):349–356.
14. MacMinn CW, Neufeld JA, Hesse MA, Huppert HE (2012) Spreading and convective dissolution of carbon dioxide in vertically confined, horizontal aquifers. *Water Resour Res* 48(11):1–11.
15. Neufeld JA, et al. (2010) Convective dissolution of carbon dioxide in saline aquifers. *Geophys Res Lett* 37(L22404):1–5.
16. Rayleigh OMFRS (1916) LIX. On convection currents in a horizontal layer of fluid, when the higher temperature is on the under side. *Philosophical Magazine Series 6* 32(192):529–546.
17. Nield DA, Bejan A (2012) *Convection in Porous Media* (Springer, Berlin), 4th Ed.
18. Riaz A, Hesse MA, Tchelepi HA, Orr FM (2006) Onset of convection in a gravitationally unstable diffusive boundary layer in porous media. *J Fluid Mech* 548:87–111.
19. Wessel-Berg D (2009) On a linear stability problem related to underground CO_2 storage. *SIAM J Appl Math* 70(4):1219–1238.
20. Slim AC, Ramakrishnan TS (2010) Onset and cessation of time-dependent, dissolution-driven convection in porous media. *Phys Fluids* 22(12):1–11.
21. Backhaus S, Turitsyn K, Ecke RE (2011) Convective instability and mass transport of diffusion layers in a Hele-Shaw geometry. *Phys Rev Lett* 106(10):104501.
22. Slim AC, Bandi MM, Miller JC, Mahadevan L (2013) Dissolution-driven convection in a Hele-Shaw cell. *Phys Fluids* 25(2):1–20.
23. Hidalgo JJ, Fe J, Cueto-Felgueroso L, Juanes R (2012) Scaling of convective mixing in porous media. *Phys Rev Lett* 109(26):264503.
24. Hewitt DR, Neufeld JA, Lister JR (2012) Ultimate regime of high Rayleigh number convection in a porous medium. *Phys Rev Lett* 108(22):224503.
25. Simmons CT, Fenstemaker TR, Sharp JM, Jr (2001) Variable-density groundwater flow and solute transport in heterogeneous porous media: Approaches, resolutions and future challenges. *J Contam Hydrol* 52(1–4):245–275.
26. Chen C, Zeng L, Shi L (2013) Continuum-scale convective mixing in geological CO_2 sequestration in anisotropic and heterogeneous saline aquifers. *Adv Water Resour* 53:175–187.
27. Elenius MT, Gasda SE (2013) Convective mixing in formations with horizontal barriers. *Adv Water Resour* 62:499–510.
28. Broadhead RF (1990) Bravo dome carbon dioxide gas field. *Treatise of Petroleum Geology, Atlas of Oil and Gas Fields, Structural Traps I*, eds Beaumont EA, Foster NH (American Association of Petroleum Geologists, Tulsa, OK), pp 213–232.
29. Broadhead RF (1993) Carbon dioxide in northeast New Mexico. *West Texas Geol Soc Bull* 32(7):5–8.
30. Pearce J, Holloway S, Wacker H (1996) Natural occurrences as analogues for the geological disposal of carbon dioxide. *Energy Convers Manage* 37(95):1123–1128.
31. Kessler JL, Soreghan GS, Wacker HJ (2001) Equatorial aridity in western Pangea: Lower permian loessite and dolomitic paleosols in northeastern New Mexico, USA. *J Sediment Res* 71(5):817–832.
32. Hennecke EW, Manuel OK (1975) Noble gases in CO_2 well gas, Harding County. *Earth* 27(2):346–355.
33. Phinney D, Tennyson J, Frick U (1978) Xenon in CO_2 well gas revisited. *J Geophys Res* 83(B5):2313–2319.
34. Ozima M, Igarashi G, Podosek F (1985) Terrestrial xenon isotope constraints on the early history of the Earth. *Nature* 315:471–474.
35. Staudacher T (1987) Upper mantle origin for Harding County well gases. *Nature* 325: 605–607.
36. Ballentine CJ, Marty B, Sherwood Lollar B, Cassidy M (2005) Neon isotopes constrain convection and volatile origin in the Earth's mantle. *Nature* 433(7021):33–38.
37. Gilfillan S, et al. (2008) The noble gas geochemistry of natural CO_2 gas reservoirs from the Colorado plateau and Rocky Mountain provinces, USA. *Geochim Cosmochim Acta* 72(4):1174–1198.
38. Cassidy M (2005) Occurrence and origin of free carbon dioxide gas deposits in the earth crust. PhD thesis (University of Houston, Houston).
39. Baines SJ, Worden RH (2004) The long-term fate of CO_2 in the subsurface: Natural analogues for CO_2 storage. *Geol Soc Lond Spec Publ* 233(1):59–85.
40. Dubacq B, et al. (2012) Noble gas and carbon isotopic evidence for CO_2-driven silicate dissolution in a recent natural CO_2 field. *Earth Planet Sci Lett* 341:10–19.
41. Dietz DN (1954) Theoretical approach to the problem of encroaching and by-passing edge water. *Proc K Ned Akad Wet* 56(B):83–93.
42. Wacker HJ, McCants SA, Sr, Cosban TJ, Allison JH, Collier JW, Sr (1995) Bravo Dome CO_2 Unit, Determination of Zero Net Pay Isopachous Line (New Mexico Oil Conservation Division), Case File No 11122.
43. Baldwin B, Muehlberger WR (1959) Geologic studies of Union County. *New Mexico: New Mexico Bureau of Mines and Mineral Resources Bulletin* 63:1–171.
44. Stroud JR (1997) The geochronology of the Raton-Clayton volcanic field, with implications for volcanic history and landscape evolution. Master's thesis (New Mexico Institute of Mining and Technology, Socorro, NM).
45. Nereson A, Stroud J, Karlstrom K, Heizler M, McIntosh W (2013) Dynamic topography of the western great plains: Geomorphic and ^{40}Ar / ^{39}Ar evidence for mantle-driven uplift associated with the Jemez lineament of NE New Mexico and SE Colorado. *Geosphere* 9(3):521–545.
46. Wolf R, Farley K, Kass D (1998) Modeling of the temperature sensitivity of the apatite (U–Th)/He thermochronometer. *Chem Geol* 148(1):105–114.
47. Hartig KA, Soreghan GS, Goldstein RH, Engel MH (2011) Dolomite in permian paleosols of the Bravo Dome CO_2 field, USA: Permian reflux followed by late recrystallization at elevated temperature. *J Sediment Res* 81(4):248–265.
48. Fessenden J, Stauffer P, Viswanathan H (2009) Natural analogs of geologic CO_2 sequestration: Some general implications for engineered sequestration. *Carbon Sequestration and Its Role in the Global Carbon Cycle*, eds McPherson BJ, Sundquist ET (American Geophysical Union, Washington, DC), pp 135–146.
49. Wackernagel H (2003) *Multivariate Geostatistics* (Springer, Berlin).
50. Vavra C, Kaldi J, Sneider R (1992) Capillary pressure: Part 5. Laboratory Methods. *ME 10: Development Geology Reference Manual*, Methods in Exploration, Vol 10 (American Association of Petroleum Geologists, Washington, DC), pp 221–225.
51. Linstrom PJ, Mallard W (2001) *NIST Chemistry Webbook; NIST Standard Reference Database no. 69*. Available at webbook.nist.gov/chemistry/. Accessed March 1, 2014.
52. Ballentine CJ, Burgess R, Marty B (2002) Tracing fluid origin, transport and interaction in the crust. Noble Gases in Geochemistry and Cosmochemistry, Reviews in Mineralogy & Geochemistry, Vol 47, eds Porcelli DP, Ballentine CJ, Wieler R (Mineralogical Society of America, Chantilly, VA), pp 539–614.
53. Criss RE (1999) *Principles of Stable Isotope Distribution* (Oxford Univ Press, New York).
54. US Environmental Protection Agency (2013) *Air Emissions*. Available at www.epa.gov/cleanenergy/energy-and-you/affect/air-emissions.html. Accessed March 3, 2014.
55. Duan Z, Sun R (2003) An improved model calculating CO_2 solubility in pure water and aqueous NaCl solutions from 273 to 533 K and from 0 to 2000 bar. *Chem Geol* 193(3–4):257–271.
56. Hewitt DR, Neufeld JA, Lister JR (2013) Convective shutdown in a porous medium at high Rayleigh number. *J Fluid Mech* 548:87–111.
57. Szulczewski ML, Hesse MA, Juanes R (2013) Carbon dioxide dissolution in structural and stratigraphic traps. *J Fluid Mech* 736:287–315.